Structural, magnetic, and Mössbauer studies of the $PrBaCuFeO_{5+y}$ compound

M. Pissas,* G. Kallias, V. Psycharis, H. Gamari-Seale, D. Niarchos, and A. Simopoulos
Institute of Materials Science, National Centre for Scientific Research Demokritos, 153 10 Ag. Paraskevi Attiki, Greece

R. Sonntag†
Berlin Neutron Scattering Center, Hahn-Meitner-Institut Glienicker Strasse 100 D-14109 Berlin, Germany
(Received 27 March 1996; revised manuscript received 4 September 1996)

We studied the structure and the magnetic properties of the oxygen deficient perovskite $PrBaCuFeO_{5+y}$ as a function of the removable oxygen y. The average crystal structure was refined from x-ray and neutron powder diffraction data which both confirm the presence of the additional oxygen y in the Pr layer. Long-range three-dimensional (3D) antiferromagnetism with $T_N = 380 \pm 5$ K was observed for the $y \approx 0$ sample and all the magnetic peaks could be indexed on two propagation vectors $\mathbf{k}_1 = [\frac{1}{2}\frac{1}{2}\frac{1}{2}]$ and $\mathbf{k}_2 = [\frac{1}{2}\frac{1}{2}1]$ from 300 to 2 K. The oxygenated sample $y \approx 0.5$ does not display magnetic reflections down to 2 K. The Mössbauer spectra of this sample display magnetic hyperfine spitting below 70 K which is attributed to spin freezing in random orientations. The hyperfine parameters of the $y \approx 0$ sample reveal two ferric iron sites ($S = 5/2$) while the oxygenated sample displays an additional iron site with higher valence. [S0163-1829(97)09101-7]

I. INTRODUCTION

Compounds with perovskite structure that are structurally and electronically related to the high-T_c superconductors present great interest. One of these compounds is $R\mathrm{BaCuFeO}_{5+y}$ (R=rare earth and Y). This oxide was found to consist of $[\mathrm{CuFeO}_{10}]_\infty$ bilayers of corner-sharing CuO_5 and FeO_5 square pyramids (Fig. 1). R^{3+} layers (coordination number 8) separate the $[\mathrm{CuFeO}_{10}]$ bilayers and accommodate the oxygen vacancies, while the Ba^{2+} ions (coordination number 12) are located within the bilayer spacing, reminiscent of the $\mathrm{YBa}_2\mathrm{Cu}_3\mathrm{O}_{6+y}$ structure.

In an earlier work[1] in order to fit the room temperature (RT) $\mathrm{YBaCuFeO}_5$ Mössbauer spectrum two crystallographically distinct Fe^{3+} sites were assumed. This assumption led them to choose the space group $P4mm$ in order to analyze the neutron powder diffraction (NPD) data. Moreover, a single crystal structural study by Voughey *et al.*[2] showed, after analysis of the data collected (hkl and hkl), that the compound is *acentric* with no observable systematic absences. Raman and IR spectra[3] for the same compound confirmed the acentric character of the unit cell. Mössbauer spectra,[4,5] at least for the $\mathrm{YBaCuFeO}_5$ compound, have shown that the initial assertion[1] for two different sites (with relative intensities 38% and 62%) must be re-examined. Crystal chemistry arguments foretell that Fe and Cu should occupy the $1b_1(z=0.27)$ and $1b_2(z=0.7)$ sites, respectively. Cu^{2+} prefers the severely elongated square pyramid, while the FeO_5 square pyramid is somewhat squashed.[6]

The magnetic properties of $\mathrm{YBaCuFeO}_{5+y}$ appear to be extremely complicated. Mössbauer and neutron diffraction data revealed an antiferromagnetic ordering transition at T_N=446 K. Moreover, the NPD data showed a magnetic phase transition at 200 K, where satellite peaks appear abruptly on either sides of the $[\frac{1}{2}\frac{1}{2}\frac{1}{2}]$ magnetic reflection.[7–9] In addition to the satellite peaks, a very small peak indexed as $(\frac{1}{2}\frac{1}{2}1)$ exists below 230 K whose intensity increases with decreasing temperature.[9]

In the case of $\mathrm{YBaCuCoO}_5$, Huang *et al.*[10] have shown that the crystal structure has the symmetry of the $P4/mmm$ space group with $a=3.8679(1)$ Å and $c=7.5674(2)$ Å. Copper and cobalt atoms are completely disordered in this compound and the oxygen vacancies are located within the yttrium layer. The magnetic structure can be described with propagation vector $\mathbf{k}=[\frac{1}{2}\frac{1}{2}\frac{1}{2}]$, $T_N=536$ K and a magnetic moment parallel to the c axis.

In a previous work[5] we have studied the $R\mathrm{BaCuFeO}_5$ series (R=Y, Nd, Sm, Gd, Dy, Tm, Lu). One series of samples (A series) was prepared by quenching from 980 °C and an-

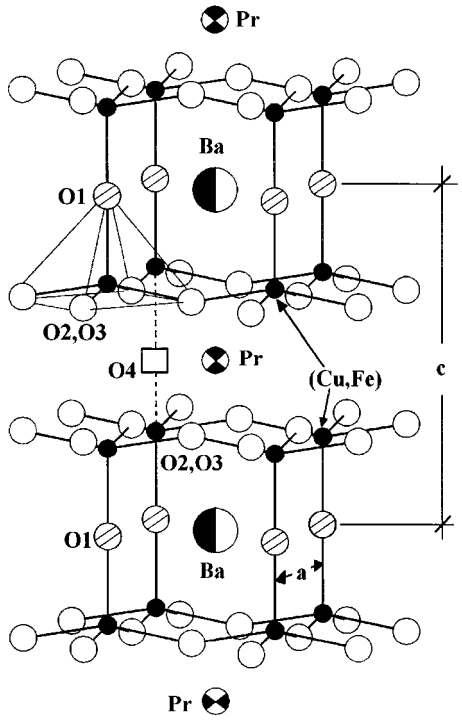

FIG. 1. Crystal structure of the $PrBaCuFeO_{5+y}$ compound.

other one (B series) was produced after deoxygenation of the A series. Heating the A series samples in an Ar atmosphere showed a weight loss that we attributed to the removal of additional oxygen within the rare earth layer. It was observed that the larger the rare earth ion, the more the weight (oxygen) loss and the increase in T_N upon deoxygenation. The A-series samples correspond to the as-prepared Pr sample studied in the present work, while the B-series samples correspond to the oxygen reduced Pr sample.

We present in this paper a detailed study of the Pr compound which, due to the large ionic radius of Pr, is expected to have a larger y value and thereby the differences in the magnetic properties as a function of oxygen should be more pronounced. The La-based compound crystallizes in the $Pm3m$ space group due to disorder between La and Ba (their ionic radii are similar) and so Pr is the largest rare earth for which the double perovskite unit cell is preserved. As it will be seen in this work, oxygen saturated samples of $PrBaCuFeO_{5+y}$ do not show any long-range magnetic order. Similar behavior has been observed[7] in the neutron diffraction patterns of the $NdBaCuFeO_{5+y}$ compound.

We have studied the $PrBaCuFeO_{5+y}$ compound using neutron, x-ray powder diffraction and Mössbauer spectroscopy data. Our main goal was to resolve the magnetic properties of this system with respect to its oxygen content.

II. EXPERIMENTAL METHODS

$PrBaCuFeO_{5+y}$ samples were prepared by thoroughly mixing high purity stoichiometric amounts of $BaCO_3$, CuO, Fe_2O_3, and Pr_6O_{11}. The mixed powders were annealed in O_2 at 980 °C for several days with intermediate grindings. Finally, the as-prepared (AP) sample was divided in two parts for further treatment. The first part—oxygen saturated sample (OS)—was annealed at 980 °C in O_2 atmosphere for two days. The second part—oxygen reduced sample (OR)—was annealed in Ar atmosphere at 500 °C for two days. Both samples were slowly cooled to RT.

The amount of extra oxygen was determined thermogravimetrically, by heating a small amount of sample in a TGA apparatus (PERKIN ELMER,TGS-2) under flowing argon at a rate of 5 °C/min up to 900 °C. Then, the sample was cooled as fast as possible to room temperature. X-ray powder diffraction (XRD) data were collected with a D500 SIEMENS diffractometer, using Cu $K\alpha$ radiation and a graphite crystal monochromator, from 4° to 120° in steps of 0.03° in 2Θ. The power conditions were set at 40 KV/35 mA. The aperture slit as well as the soller slit were set at 1°. The neutron powder diffraction experiments were performed in the flat-cone diffractometer E2 of the research reactor BERII in Berlin. The (311) reflection of the Ge monochromator with wavelength $\lambda = 1.2$ Å and the (002) reflection of pyrolytic graphite monochromator with wavelength $\lambda = 2.4$ Å were used. dc magnetization measurements were performed in a superconducting quantum interference device (SQUID) magnetometer (Quantum Design). The absorption Mössbauer spectra were recorded using a conventional constant acceleration spectrometer with $^{57}Co(Rh)$ source moving at RT, while the absorber was kept fixed each time at the desired temperature. The spectra at temperatures above RT were taken in a furnace with a temperature stability of 0.1 K. The resolution and the calibration of the spectrometer were made at RT using an α-Fe foil as the absorber. The resolution was determined to be $\Gamma/2 = 0.14$ mm/s.

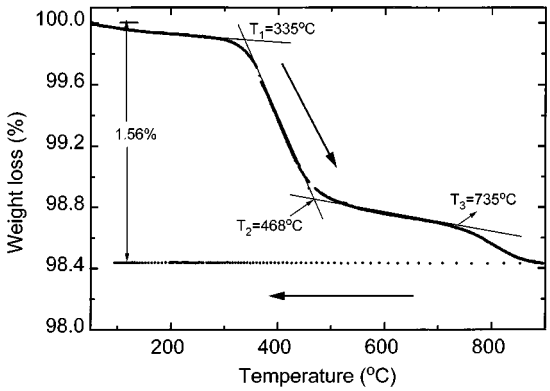

FIG. 2. The TGA trace for the oxygen saturated $PrBaCuFeO_{5+y}$ compound after heating in flowing Ar up to 900 °C at a rate of 4 °C.

III. THERMOGRAVIMETRIC MEASUREMENTS

Figure 2 shows the TGA trace for the OS sample. The sample starts to lose oxygen near 335 °C, in close similarity to the 123 compound,[11] and at 468 °C it loses almost 1.2%. Then, almost up to 760 °C the rate of oxygen loss is practically negligible. Finally, from 735 °C up to 900 °C it loses another 0.3%. In order to calculate the amount of extra oxygen we assumed that at the end of this procedure the sample had exactly five oxygen atoms per unit cell (such as the OR sample), that is, $PrBaCuFeO_5$. In this way, the amount of extra oxygen was estimated to be $y \approx 0.47 \pm 0.02$. Similar TGA trace has also been observed for the AP sample. In that case, the extra oxygen was estimated to be $y \approx 0.26 \pm 0.04$.

IV. STRUCTURAL X-RAY AND NEUTRON POWDER DIFFRACTION STUDY

All the reflections within the resolution of the x-ray diffractometer were indexed in a tetragonal unit cell. The fact that no conditions of reflections were observed leads to eight possible space groups $P4/mmm$, $P4mm$, $P422$, $P\bar{4}2m$, $P\bar{4}m2$, $P4/m$, $P4$, and $P\bar{4}$, with $P4/mmm$ being the only centrosymmetric one. The similarity of the x-ray powder pattern with that of the $YBaCuFeO_5$ compound led us to describe the structure with a similar model. Taking Ba at the origin (0,0,0), the atomic positions in the case of $P4mm$ can be described in terms of seven parameters: δz_{Pr}, z_{Fe}, z_{Cu}, δz_{O1}, z_{O2}, z_{O3}, and δz_{O_4}. Then the coordinates of the various atoms are Ba at (0,0,0), Pr at $(0,0,\frac{1}{2}+\delta z_{Pr})$, Fe at $(\frac{1}{2},\frac{1}{2},z_{Fe})$, Cu at $(\frac{1}{2},\frac{1}{2},z_{Cu})$, O1 at $(\frac{1}{2},\frac{1}{2},\delta z_{O1})$, O2 at $(\frac{1}{2},0,z_{O2})$, O3 at $(\frac{1}{2},0,z_{O3})$, and O4 at $(\frac{1}{2},\frac{1}{2},\delta z_{O4})$. The O4 oxygen was introduced as the only possible solution for the removable oxygen that was observed in the thermogravimetry experiments. The atoms are identified as shown in Fig. 1. Therefore, these atomic coordinates together with the occupancy of the O4 sites and the twenty-four anisotropic temperature parameters give the whole picture of the structure (hereafter Model I).

For the $P4/mmm$ space group, it is $z_{Fe}=z_{Cu}$, $z_{O2}=z_{O3}$, $\delta z_{O1}=0$, $\delta z_{Pr}=0$, and $\delta z_{O4}=0$ (hereafter Model II). A third model (Model III) was introduced for $YBaCuFeO_5$ from Caignaert *et al.*[9] Namely, it is the same with (Model II) except that, $z_{Fe}\neq z_{Cu}$. As we will see in the next section the analysis of the magnetic reflections for the OR sample sets a strong constrain in the structural model, at least for this sample. Therefore, we will discuss the structure of the OR and OS samples only within models II and III.

The refinement of the XRD patterns was carried out by the BBWS-9006 Rietveld program,[12] while for the NPD patterns we used the FULLPROF program.[13] The refinements obtained for the OS and OR samples using NPD data at RT are shown in Fig. 3. The resulting fitting parameters for the XRD and NPD data are given in Tables I and II. The shape of the peaks was assumed to be Pearson VII for the x rays and pseudo-Voigt for the neutrons. The background was refined together with the structure for the x rays, while for the neutrons it was estimated by interpolation between regions of the profile where no reflections were observed. In order to compare the results of models II and III we used the same isotropic thermal parameters. The values obtained from the neutron data refinement are more reliable. In the OR sample it is worth to mention the increase of the $|z_{Fe}-z_{Cu}|$ value with respect to the OS sample. This result is hard to be deduced from the x ray data due to the similarity in the scattering factors of Cu and Fe.

The quality of the x-ray refinement was appreciably higher when we introduced the extra oxygen O4 (R_B decreased from 4.90% to 2.97%). In the case of the neutron data, the improvement due to the introduction of O4 was dramatic and only then the refinement converged. Moreover, there are several differences in the neutron patterns between OS and OR, which originate from the extra O4 oxygen atoms. For example, the peak at $2\theta=20°$ in the pattern of the OR sample (Fig. 3) comes implicitly from the oxygen deficiency at the O4 sites. From the neutron data the occupancy of O4 oxygen atoms was refined to 0.49(1), that is in close agreement with the 0.57(2) value obtained from the x-ray data. It is remarkable that the refinement of the x-ray data for the AP and OS samples gave occupancies for the O4 atoms that are not far from the value deduced from thermogravimetry.

The refinement of the x-ray data showed that model I, for both OR and OS samples, has a slightly lower R_B, but there is violation of the principle of *minimum assumption.*[14] On the other hand, the NPD data show that model III, for both OR and OS samples, has a slightly lower R_B and is within the principle of minimum assumption. Consequently, if we accept that the principle of *minimum assumption* plays an important role and since NPD is more reliable than XRD in determining the correct structure model, then a reasonable structural description can be given with model III.

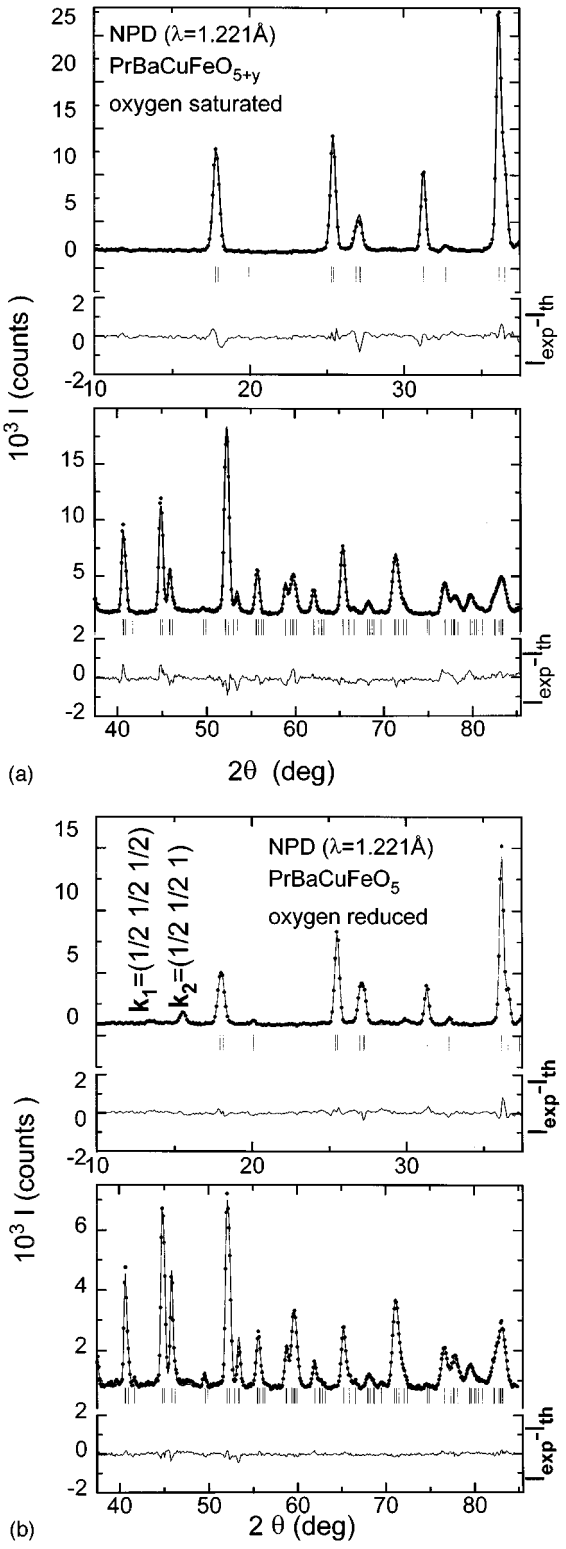

FIG. 3. Rietveld refinement patterns at RT for the (a) OS and (b) OR $PrBaCuFeO_{5+y}$ samples using neutron powder diffraction data ($\lambda=1.221$ Å). The observed intensities are shown by dots and the calculated ones by the solid line. The positions of the Bragg reflections are shown by the small vertical lines below the pattern. The line at the bottom indicates the intensity difference between the experimental and the refined patterns.

V. MAGNETIC STRUCTURE

Figure 4 shows the neutron diffraction patterns of the OS and OR samples at 2 K. For the OS sample no magnetic reflection is observed down to 2 K, while for the OR sample there are two families of peaks in addition to the nuclear ones. Similar behavior with the OS sample was observed for

TABLE I. Fractional atomic coordinates, isotropic temperature factors, occupancy factors for the oxygen saturated and the oxygen reduced $PrBaCuFeO_{5+y}$ samples using x-ray powder diffraction data. Rietveld refinements were done in the tetragonal space groups $P4mm$ (model I), $P4/mmm$ (model II) and $P4/mmm$, with $z_{Fe} \neq z_{Cu}$ (model III). Atom positions are Pr(0,0,z), Ba(0,0,0), Fe(1/2,1/2,z), Cu(1/2,1/2,z), O1(1/2,1/2,z), O2(1/2,0,z), O3(1/2,0,z), O4(1/2,1/2,1/2). The occupancy of O4 (y) was found to be 0.57(2) and 0 for the OS and OR samples, respectively.

	Oxygen saturated $a=3.9219(1)$ Å[a] $c=7.7558(5)$ Å				Oxygen reduced $a=3.9260(1)$ Å $a=7.7669(7)$ Å			
Atom	I	II	III	B	I	II	III	B
	z	z	z		z	z	z	
Ba	0	0	0	0.55(7)	0	0	0	0.70(5)
Pr	0.502(2)	1/2	1/2	0.68(7)	0.507(1)	1/2	1/2	0.36(5)
Fe	0.252(1)	0.2617(5)	0.249(1)	0.50(1)	0.253(1)	0.2620(5)	0.244(1)	0.45(3)
Cu	0.732(1)	0.2617(5)	0.270(1)	0.50(1)	0.734(1)	0.2620(5)	0.272(1)	0.45(3)
O1	0.017(5)	0	0 0	1.3(1)	-0.002(6)	0	0	0.6(1)
O2	0.306(4)	0.292(1)	0.292(1)	1.3(1)	0.324(2)	0.302(1)	0.303(1)	0.6(1)
O3	0.725(6)		0.	1.3(1)	0.718(3)			0.6(1)
O4	1/2	1/2	1/2	1.3(1)	1/2	1/2	1/2	0.6(1)
R_p	5.05	5.07	5.01		5.90	5.97	5.79	
R_wp	7.69	7.71	7.69		7.35	7.42	7.30	
R_B	2.97	3.02	3.06		4.31	4.48	4.54	

[a]For the AP sample the cell constants are $a=3.9234$ Å and $c=7.7622$ Å.

the as-prepared $NdBaCuFeO_{5+y}$ compound, where $y \neq 0$.[7] The same peaks exist in the NPD pattern at RT, but not in the XRD pattern for the same sample, and since their intensity decreases with increasing temperature these peaks can be attributed to magnetic long-range order.

The magnetic peaks can be indexed with superlattice indices $(h_1/2,k_1/2,l_1/2)$ and $(h_2/2,k_2/2,l_2)$, where h_1, k_1, h_2, k_2, l_1, l_2 are odd integers. The first family of magnetic reflections with indices $(h_1/2,k_1/2,l_1/2)$ comes from a spin arrangement with propagation vector $\mathbf{k}_1=[\frac{1}{2},\frac{1}{2},\frac{1}{2}]$. The half-integer indices imply that $\mathbf{S}(\mathbf{R}+\mathbf{c})=-\mathbf{S}(\mathbf{R})$ and

TABLE II. Fractional atomic coordinates, isotropic temperature factors, occupancy factors for the oxygen saturated and oxygen reduced $PrBaCuFeO_{5+y}$ samples using neutron powder diffraction data. Rietveld refinements were done in the tetragonal space groups $P4mm$ (model I), $P4/mmm$ (model II) and $P4/mmm$ with $z_{Fe} \neq z_{Cu}$ (model III). Atom positions are Pr(0,0,z), Ba(0,0,0), Fe(1/2,1/2,z), Cu(1/2,1/2,z), O1(1/2,1/2,z), O2(1/2,0,z), O3(1/2,0,z), O4(1/2,1/2,1/2). The occupancy of O4 (y) was found to be 0.49(1) and 0.04(1) for the OS and OR samples, respectively.

	Oxygen saturated $a=3.9219$ Å[a] $c=7.7558$ Å				Oxygen reduced $a=3.9260$ Å $a=7.7669$ Å			
Atom	I	II	III	B	I	II	III	B
	z	z	z		z	z	z	
Ba	0	0	0	0.58(6)	0	0	0	0.78(5)
Pr	0.494(2)	1/2	1/2	0.58(6)	0.496(3)	1/2	1/2	0.37(5)
Fe	0.255(4)	0.2580(3)	0.254(2)	0.53(4)	0.246(2)	0.2596(3)	0.2448(6)	0.18(2)
Cu	0.741(4)	0.2580(3)	0.262(3)	0.53(4)	0.728(2)	0.2596(3)	0.2770(7)	0.18(2)
O1	-0.011(5)	0	0 0	1.2(2)	-0.008(4)	0	0	1.1(1)
O2	0.280(5)	0.2915(3)	0.2915(3)	1.8(1)	0.292(3)	0.3040(5)	0.3047(1)	0.9(1)
O3	0.698(6)	-	-	1.8(1)	0.684(3)	-	-	0.9
O4	0.49(1)	1/2	1/2	0.4(3)	-	1/2	1/2	0.9
R_p	4.18	4.21	4.13		4.96	5.04	4.56	
R_wp	5.30	5.39	5.28		6.31	6.26	5.82	
R_B	6.48	6.25	6.22		5.49	6.71	4.75	

[a]Due to possible errors in the neutron wavelength, which is the largest source of the absolute error in the determination of the lattice parameters, we kept the cell constants equal to those determined from the x rays and refined only the zero position and the neutron wavelength.

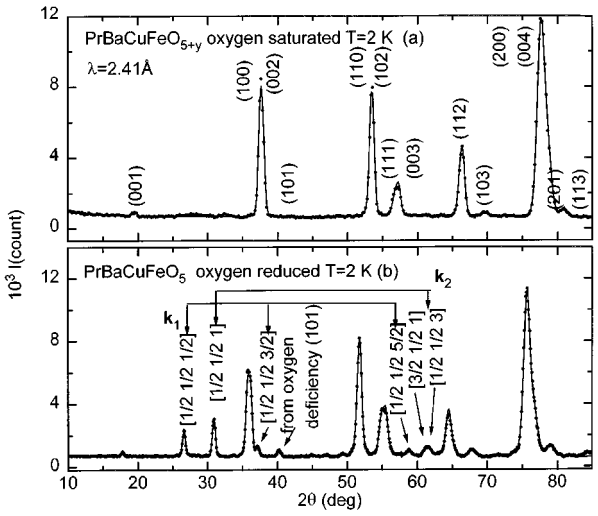

FIG. 4. Rietveld refinement patterns at 2 K for the (a) OS and (b) OR $PrBaCuFeO_5$ samples using neutron powder diffraction data ($\lambda = 2.41$ Å). The observed intensities are shown with dots and the calculated ones with the solid line. The solid line across the magnetic peaks of the OR sample is calculated by using the intensities of Table III and by assuming the same profile and scale factor as for the nuclear peaks.

$\mathbf{S}(\mathbf{R}+\mathbf{a}) = -\mathbf{S}(\mathbf{R})$ [or $\mathbf{S}(\mathbf{R}) = \exp(i\mathbf{k}_1\cdot\mathbf{R})\mathbf{S}(\mathbf{0})$], where $\mathbf{R}$ is a lattice vector and $\mathbf{S}(\mathbf{R})$, $\mathbf{S}(\mathbf{0})$ are the magnetic moments at the lattice sites $\mathbf{R}$ and $\mathbf{0}$, respectively. The second family of magnetic reflections with indices $(h_2/2, k_2/2, l_2)$ comes from a spin arrangement with propagation vector $\mathbf{k}_2 = [\frac{1}{2}, \frac{1}{2}, 1]$, which implies that $\mathbf{S}(\mathbf{R}+\mathbf{c}) = \mathbf{S}(\mathbf{R})$ and $\mathbf{S}(\mathbf{R}+\mathbf{a}) = -\mathbf{S}(\mathbf{R})$. According to the above remarks three are the possible candidate collinear magnetic models for $\mathbf{k}_1$ and only one for $\mathbf{k}_2$. These models are illustrated in Fig. 5.

Since the half-integer and integer Bragg reflections correspond to separate Fourier components they can be treated separately. We may then solve the components of the spin structure for the two types of reflections separately. The observed reflections can be interpreted with two models: (a) an *incoherent mixture of domains* with different propagation vectors and with the same ordered moment, but occupying different volumes and (b) a *canted model* which is the vector sum of two collinear magnetic structures with different ordered magnetic moments but occupying the same volume.[15] The integrated intensity of a magnetic reflection for a collinear magnetic structure in a NPD pattern can be written as:

$$I(hkl) = \frac{I_0}{v_{om}^2}\frac{1}{\sin\theta\sin 2\theta} m\langle 1-(\hat{\mathbf{q}}\cdot\hat{\mathbf{s}})^2\rangle_{\{hkl\}}|F(hkl)|^2, \tag{1}$$

where I_0 is the scale factor, v_{0m} is the volume of the magnetic unit cell, θ is the Bragg angle and m is the multiplicity of the plane hkl. The term $\langle 1-(\hat{\mathbf{q}}\cdot\hat{\mathbf{s}}^2\rangle_{\{hkl\}}$ is an average over all the equivalent $\{hkl\}$ reflections, $\hat{\mathbf{q}}$ is the unit vector along the scattering vector, $\hat{\mathbf{s}}$ is the unit vector along the axis of the colinear magnetic structure and $F(hkl)$ is the magnetic structure factor. From NPD data in a magnetic structure with tetragonal configuration symmetry we can calculate only the magnitude of the magnetic moment and the angle with the tetragonal axis. Taking into account the above remarks, the magnetic structure factor for a magnetic unit cell with constants $a_M = b_M = \sqrt{2}a_N$, $c_M = 2c_N$ which correspond to the $\mathbf{k}_1$ is

$$F(hkl) = (1-e^{\pi i(h+k)})(1-e^{\pi il})(p_A e^{2\pi ilz} + e^{\pi il} p_B e^{-2\pi ilz}), \tag{2}$$

where $p_j = (\text{occupancy})\times(0.269\times 10^{-12}\text{cm}/\mu_B)\times S_j \times f_j \times \exp(-W_j)$, S_j is the average ordered magnetic moment (in Bohr magnetons μ_B) for the jth atom in the j layer ($j = A, B$), f_j is the magnetic form factor[16] for the magnetic ion at the jth layer and W_j is the Debye-Waller factor for the jth atom. Similarly, the structure factor for the reflections

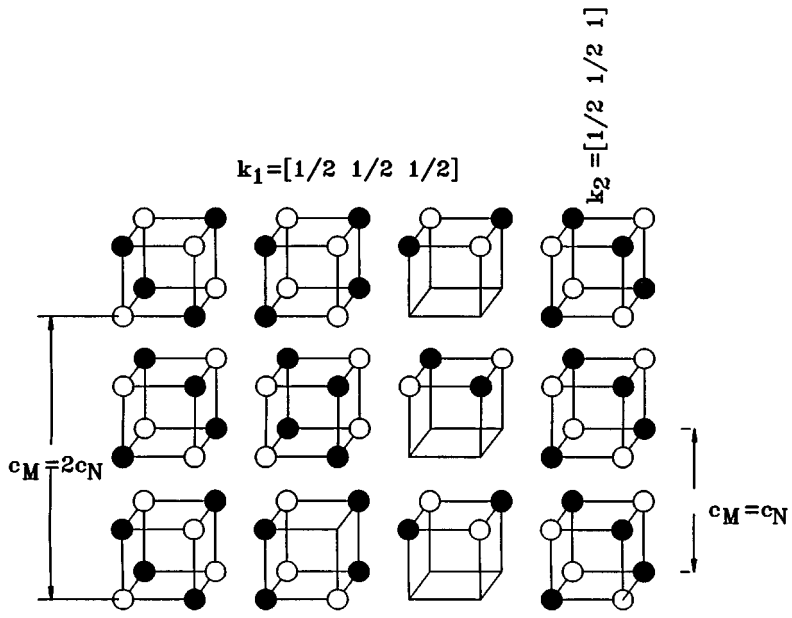

FIG. 5. The possible collinear magnetic structures for the $\mathbf{k}_1$ and $\mathbf{k}_2$ propagation vectors. Filled and open circles represent spin down and spin up, respectively.

TABLE III. Comparison between the observed I_{obs} and the calculated I_{calc} integrated intensities of the observed magnetic reflections for the OR $PrBaCuFeO_5$ compound at 4.2 K within the canted model. Fe^{3+} and Cu^{2+} are occupying the site with $z=0.25$. The I_{obs} were extracted from the experimental data by using as peak shape function the same with the one used for the nuclear structure analysis. The I_{cal} were calculated by using Eq. (1).

$k_1=[\frac{1}{2}\frac{1}{2}\frac{1}{2}]$				
hkl	I_{obs} (arb. units)	$I_{cal}(\mathbf{S}\perp c)$	$I_{cal}(\mathbf{S}\parallel c)$	$I_{cal}(\mathbf{S})$
$\frac{1}{2}\frac{1}{2}\frac{1}{2}$	996±10	708	1084	958
$\frac{1}{2}\frac{1}{2}\frac{3}{2}$	320±10	484	280	336
$\frac{1}{2}\frac{1}{2}\frac{5}{2}$	96±10	208	56	100
S_{1x} [a]		1.45(1)	0.0	0.7(1)
S_{1z}		0.0	1.41(1)	1.18(1)
S_1 [b]		1.45(2)	1.41(1)	1.41(1)
R_B		40%	11%	2%
$k_2=[\frac{1}{2}\frac{1}{2}1]$				
hkl	I_{obs}	$I_{cal}(\mathbf{S}\perp c)$	$I_{cal}(\mathbf{S}\parallel c)$	$I_{cal}(\mathbf{S})$
$\frac{1}{2}\frac{1}{2}1$	1404±5	1384	1372	
$\frac{3}{2}\frac{1}{2}1$	472±5	412	688	
$\frac{1}{2}\frac{1}{2}3$	384±5	332	64	
S_{2x}		1.53(2)	0.0	
S_{2z}		0.0	1.53(2)	
S_2 [c]		1.53(2)	1.53(2)	
R_B		5.6%	25%	

[a]Due to the tetragonal configuration symmetry we suppose that S_{ab} is along the x and y axis for the propagation vectors $\mathbf{k}_1$ and $\mathbf{k}_2$, respectively.

[b]$S_1=\sqrt{S_{1x}^2+S_{1z}^2}$ (ordered moment per ion for the $\mathbf{k}_1$ magnetic structure).

[c]$S_2=\sqrt{S_{2x}^2+S_{2z}^2}$ (ordered moment per ion for the $\mathbf{k}_2$ magnetic structure).

which correspond to the $\mathbf{k}_2$ propagation vector supposing a magnetic unit cell with cell constants $a_M=b_M=\sqrt{2}a_N$, $c_M=c_N$ is

$$F(hkl)=(1-e^{\pi i(h+k)})(p_A e^{2\pi i l z_A}+p_B e^{-2\pi i l z_B}). \quad (3)$$

For $\mathbf{k}_2$ the absence of the magnetic Bragg peak with $l=0$ implies that the summation of the spins of two adjacent layers is zero which means that the magnetic moment of these layers is of equal magnitude but in opposite directions ($p_A=-p_B$). This fact can be realized only if the layers A and B are equivalent. Consequently $z_B=1-z_A$ and the structure factor takes the final form

$$F(hkl)=(1-e^{\pi i(h+k)})2ip_A\sin(2\pi lz). \quad (4)$$

Since we have a large number of parameters and a small number of magnetic reflections it would be difficult to adopt two kinds of magnetic ions having different moments. For this reason we considered that the magnetic ions occupy the $z=0.25$ position and that they are represented by a mean magnetic moment. With this simplification, basically we use the structural description based on model II in order to analyze the magnetic reflections. On the other hand, we must note that there might be an error in the estimation of the mean magnetic moment, but the small contribution of the Cu^{2+} moment does not alter appreciably the final result. To determine the magnetic structure, integrated intensity data from various reflections were compared to those calculated from several spin models. Finally in Table III we summarize the results of the analysis of the magnetic reflections.

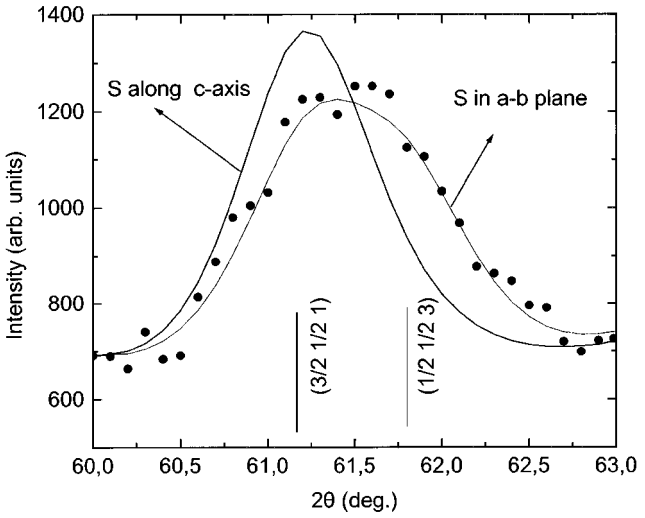

FIG. 6. $(\frac{3}{2}\frac{1}{2}1)$ and $(\frac{1}{2}\frac{1}{2}3)$ peaks of the 2 K-NPD pattern of the OR $PrBaCuFeO_{5+y}$ sample. The solid lines were calculated by assuming that $S\perp c$ and $S\parallel c$ axis, respectively.

A. Analyses of the $\mathbf{k}_1$ propagation vectors peaks

For the magnetic structure that is described by $\mathbf{k}_1$ there are two possibilities $p_A=p_B$ or $p_A=-p_B$. The difference in the calculated patterns between the two models is negligible [because according to Eq. (2) for $z\approx\frac{1}{4}$, $F^2\propto 4p_A^2\sin^2(\pi/4)$ or $F^2\propto 4p_A^2\cos^2(\pi/4)$ for $p_A=p_B$ or $p_A=-p_B$, respectively], so we cannot distinguish between them. The calculation with the magnetic moment lying in the ab plane gave poor agreement. A better result was obtained by assuming that the magnetic moment is directed along the c axis. Moreover, if the magnetic moment had one component along the c axis and the other in the ab plane, the agreement was significantly improved ($R_M=2\%$). This result can be extracted when we compare the intensity ratio between the peaks (1/2 1/2 3/2) and (1/2 1/2 1/2), which depends only on the orientation factor $\langle 1-(\hat{\mathbf{q}}\cdot\hat{\mathbf{s}})^2\rangle_{\{hkl\}}$ and not on the size of the magnetic moment.

B. Analyses of the $\mathbf{k}_2$ propagation vectors peaks

The parameters we have to estimate for the magnetic structure described with $\mathbf{k}_2$ is the size of the magnetic moment and the angle with respect to the c axis. Although we have only three reflections available, there is a point which plays an important role in the determination of the angle between the magnetic moment and the c axis. If we compare the calculated and experimental patterns of the partially resolved reflections (3/2 1/2 1) and (1/2 1/2 3) (see Fig. 6), the agreement is better with the spins lying in the ab plane than along the c axis.

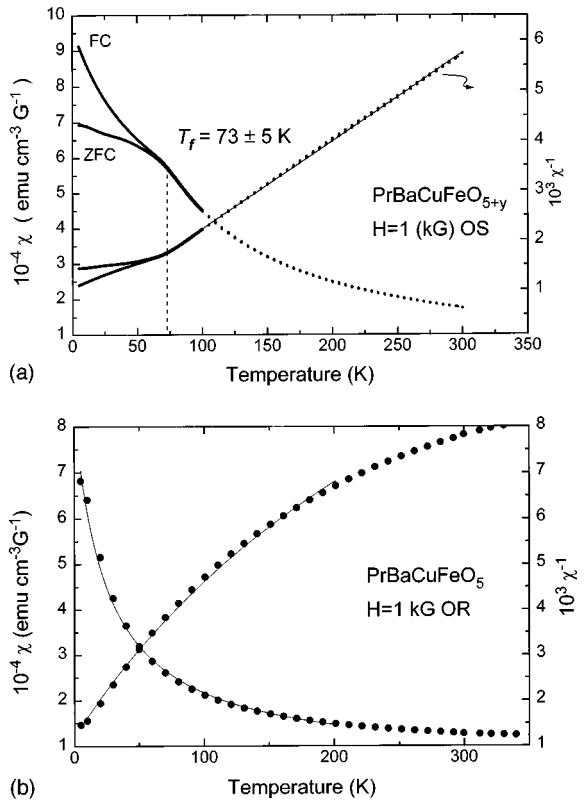

FIG. 7. Temperature dependence of the magnetic susceptibility for the (a) OS and (b) OR PrBaCuFeO$_{5+y}$ sample in both zero field and field cooling modes. The measurements were performed in an applied magnetic field of 1 kG.

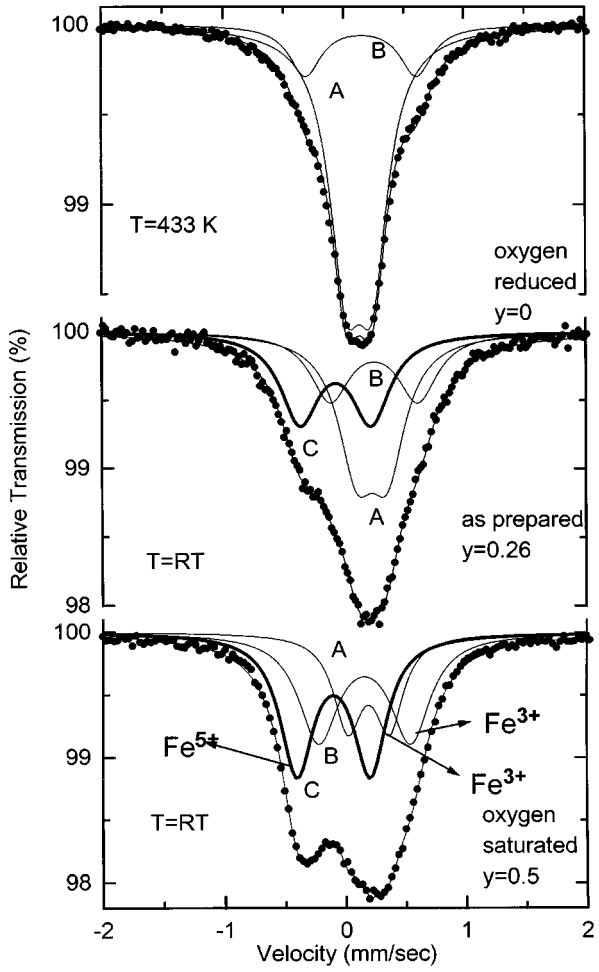

FIG. 8. Mössbauer spectra for the OR sample ($y\approx 0$) at 433 K, for the AP sample ($y\approx 0.26$) at RT and for the OS sample ($y\approx 0.5$) at RT.

Based on the above arguments, for the canted magnetic structure model the ordered magnetic moments per ion at 2 K are estimated to be $S[\mathbf{k}_1]=1.34\ \mu_B$ $[\mathbf{S}(\mathbf{k}_1)=0.7\hat{\mathbf{x}}+1.18\hat{\mathbf{z}}]$ and $\mathbf{S}[\mathbf{k}_2]=1.57\hat{\mathbf{y}}\ \mu_B$. The same analysis can be applied at 100, 200, and 300 K, yielding $S[\mathbf{k}_1]=\{1.27,\ 1.09,\ \ 0.75\}\ \mu_B$ and $S[\mathbf{k}_2]=\{1.53,\ 1.43,\ 1.17\}\ \mu_B$, respectively. For the model with the incoherent mixture of domains with the two propagation vectors having the same ordered moment ($S\approx 2\ \mu_B$), the two domains $\mathbf{k}_1$ and $\mathbf{k}_2$ occupy 41% and 59% of the total volume of the crystal at 2 K, respectively.

VI. MAGNETIZATION MEASUREMENTS

Figure 7(a) shows the χ vs T curve of the OS sample for an applied field of 1 kG. The zero field cooling (ZFC) measurement exhibits a change in the slope at 73 ± 5 K, while the field-cooling (FC) branch does not coincide with the ZF branch below this temperature. This kind of anomaly, as the NPD data have shown, does not correspond to an antiferromagnetic long-range order. Such an anomaly can be attributed to the freezing of the magnetic moments in the time scale of the measurement with the SQUID magnetometer.

The data were analyzed using the modified Curie-Weiss equation $\chi=C/(T-\Theta)+\chi_0$ with C being given by the relation $C=\mu_{\rm eff}^2 N/3k_B$, where N is the number of magnetic ions per unit volume, $\mu_{\rm eff}$ is the effective magnetic moment and k_B is the Boltzman constant. For the OS sample, $N=3$ (Cu, Fe, and Pr). The parameters χ_0, C, and Θ were determined by a least-squares fitting in the range 73–300 K and for $H=1$ kG. From the estimated value of $C=0.057\pm 0.001$ emu cm^{-3}Øe^{-1}K^{-1}, we calculated the effective magnetic moment $\mu_{\rm eff}=3.32\mu_B$ per magnetic ion and $\Theta\approx -22$ K. The negative value of Θ indicates antiferromagnetic correlations between the magnetic moments. Assuming that Fe has $S=5/2$, Cu has $S=1/2$ and that for Pr^{3+} it is $J=4$, $L=5$, $S=1$, the effective magnetic moment is $\mu_{\rm eff}=3.70\ \mu_B$ per ion, that is very close to the observed value. The difference may come from the fact that not all Fe ions have $S=5/2$ (e.g., Fe^{5+} has $S=3/2$).

The magnetic susceptibility curve for the OR sample (from 4.2 to 350 K) is shown in Fig. 7(b). Because of the limitations of our magnetometer we were not able to observe the antiferromagnetic transition which, according to the Mössbauer results, occurs near 380 K. Least-squares fitting in the range 5–200 K gives for the paramagnetic contribution a $\mu_{\rm eff}=3.18\ \mu_B$ per magnetic ion and $\Theta=-20$ K. For this case $N=1$ (Pr), since Cu and Fe do not contribute to the paramagnetic moment (they are antiferromagnetically ordered). The value of $\mu_{\rm eff}$ is close to that of $Pr^{+3}[J=4,\ L=5,\ S=1,\ \mu_{\rm eff}(Pr^{+3})=g\sqrt{J(J+1)}=3.58]$.

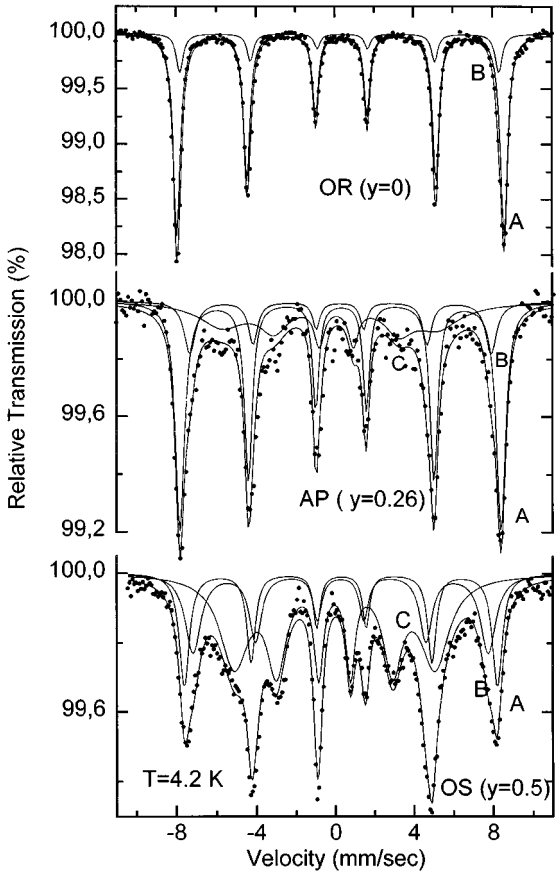

FIG. 9. Mössbauer spectra for the OR ($y\approx 0$), AP ($y\approx 0.26$), and OS ($y\approx 0.5$) $PrBaCuFeO_{5+y}$ samples at 4.2 K.

This result supports the exclusion of the Pr sublattice from the analysis of the magnetic reflections for the OR sample.

VII. MÖSSBAUER SPECTRA

Figure 8 shows the RT Mössbauer spectra of the OS, AP samples and the 433 K spectrum of the OR sample in the paramagnetic region, whereas the 4.2 K spectra are shown in Fig. 9. The parameters obtained from the least-squares fit for all the samples are listed in Table IV.

The 433 K spectrum of the OR sample was analyzed with two components, namely *A* and *B* (for labelling see Table IV). Their isomer shift values are typical of Fe^{3+} in the high spin state ($S=5/2$). The presence of two components in the spectra is unexpected since our structural model contains only one crystallographic position for Fe. An account for the occurrence of two sites will be given in the discussion section. As the temperature is lowered, near 380 K the two doublets start to collapse and in this way the T_N for the OR sample is estimated as $T_N=380\pm 5$ K. The RT spectrum of the OR sample exhibits an inhomogeneous broadening such as in the case of the $YBaCuFeO_5$ compound or the other members of the $RBaCuFeO_5$ series.[5,4] At 4.2 K the spectrum consists of two components whose linewidth is close to the instrumental resolution ($\Gamma/2\approx 0.14$ mm/s). A small inhomogeneous broadening is present and can be described phenomenologically with a Lorentzian distribution of the hyperfine field. The hyperfine field values for both sites confirm the identification of ferric iron in the high spin state.

The principal axis of the electric field gradient tensor is along the *c* axis and supposing that $\eta=0$ (an assumption supported by the tetragonal symmetry) and that $q=V_{zz}/e$ is positive (as indicated from point charge calculation of V_{zz}), we can deduce the angle between the iron magnetic moment $\langle \mathbf{S} \rangle$ and the *c* axis from the values of ϵ at 433 K and 4.2 K (for both components *A* and *B*). The result is $\theta_A=60^\circ\pm 2^\circ$ and $\theta_B=61^\circ\pm 2^\circ$, that is $\theta_A\approx\theta_B$.

The spectra of the OS sample appear to be more complicated. The RT spectrum shows an asymmetry, while the 4.2 K spectrum was adequately fitted with three sextets. The first two have magnetic hyperfine fields and isomer shifts that are both indicative of ferric iron in the high spin ($S=5/2$) state. The third sextet with $H\sim 316$ kG and $\delta=0.07$ mm/s, nonexistent in the spectrum of the OR sample, can be related to the extra oxygen that is inserted in the unit cell as judged from its relative spectral area ($45\%\pm 5\%$) and the occupancy of the O4 ($x\approx 0.5$). Based on the 4.2 K spectrum we fitted the paramagnetic RT spectrum with three doublets.

Spectra were also taken at 40, 70, and 100 K, in order to see the effect of the susceptibility anomaly near 70 K to the Mössbauer spectra. At 70 K (Fig. 10) we observed a broad unresolved spectrum which could originate from a distribution, or relaxation of hyperfine magnetic field, while at 100 K the spectrum is paramagnetic. At 40 K the spectrum is just like the one at 4.2 K. Therefore, the Mössbauer spectra follow closely the susceptibility anomaly at 70 K.

The AP sample is expected to represent an intermediate situation between the OR and OS samples. Indeed, we observe an increase in the intensity of component A with respect to the OS sample. At 4.2 K all three components are magnetically split. The relative area of the *C* component is related to the extra oxygen if we take into consideration the amount of the extra oxygen, which is $x=0.26$ for this sample.

VIII. DISCUSSION

Before discussing the crystal chemistry of $PrBaCuFeO_5$, we would like to notice that the positions for Cu, Fe, and O(2) in the OS sample obtained from x-ray and neutron diffraction data are averaged over several oxygen coordination numbers. The observed coordination polyhedron around Cu and Fe is an average over microscopic configurations depending on whether the O4 site is occupied or not.

Let us now discuss the changes that are caused in the unit cell by the removal of oxygen and try to connect them with the differences in the calculated bond valence sums (BVS). We have calculated the bond valence sums for the various atoms in the $PrBaCuFeO_{5+y}$ structure using the relation $V_i=\Sigma_j \exp[(r_o-r_{ij})/B]$ where the sum is over all the nearest neighbors, $B=0.37$, $r_o(Fe^{3+}-O^{2-})=1.759$, $r_o(Cu^{2+}-O^{2-})=1.679$, $r_o(Cu^{3+}-O^{2-})=1.730$, $r_o(Ba^{2+}-O^{2-})=2.285$, $r_o(Pr^{3+}-O^{2-})=2.138$ and r_{ij} is the bond length between the *i* and *j* ions.[17] The BVS calculations were performed for the case of models II and III using the cation-oxygen distances that were deduced from the refinement of NPD patterns. The results are nearly identical, for

TABLE IV. Experimental values of the half linewidth $\Gamma/2$ in mm/s, the isomer shift δ relative to metallic Fe at RT in mm/s, the quadrupole shift ε in mm/s, the hyperfine magnetic field H in kG, the HWHM ΔH of the hyperfine magnetic field Lorentzian distribution which modulates the line widths, as obtained from least-squares fits of the Mössbauer spectra of the OS, AP, and OR $PrBaCuFeO_{5+y}$ samples. ε denotes the eigenvalues of the Hamiltonian of the quadrupole interaction or of the quadrupole perturbation that are given by the relations $\varepsilon=(1/4)e^2qQ(1+\eta^2/3)^{1/2}$ and $\varepsilon=(1/8)e^2qQ(3\cos^2\theta-1+\eta\sin^2\theta\cos2\phi)$ for the paramagnetic and the magnetic case, respectively. A_i is the relative intensity. The numbers in parentheses are estimated standard deviations referring to the last significant digit.

T	Site	$\Gamma/2$	δ	ϵ	H	ΔH	A_i
OR	$y\approx0$						
433	*A*	0.16(1)	0.219(1)	0.110(1)			83(1)
	B	0.16(0)	0.241(4)	0.446(4)			17(1)
300	*A*	0.15	0.311(5)	-0.011(4)	322(1)	33(1)	87(5)
	B	0.15	0.318	-0.069	298(3)	33(2)	13(5)
4.2	*A*	0.171(1)	0.430(1)	-0.013(1)	515(1)	3(5)	85(4)
	B	0.171(1)	0.436(1)	-0.069(7)	509(1)	2(3)	15(4)
AP	$y\approx0.26$						
300	*A*	0.18(1)	0.331(6)	0.128(7)			43(3)
	B	0.19(1)	0.35(1)	0.36(1)			25(4)
	C	0.19(1)	0.03(1)	0.295(4)			32(3)
4.2	*A*	0.18	0.409	-0.01	506(1)	6	55(3)
	B	0.19	0.384	-0.01	475(1)	9	15(7)
	C	0.19(1)	0.01(1)	-0.16(5)	346(6)	70(2)	29(11)
OS	$y\approx0.5$						
300	*A*	0.140(6)	0.295(5)	0.172(5)			23(2)
	B	0.172(5)	0.262(8)	0.382(5)			36(3)
	C	0.166(4)	0.003(4)	0.304(1)			41(2)
4.2	*A*	0.18(1)	0.409(5)	-0.009(5)	493(1)	5(1)	23(3)
	B	0.23(1)	0.384(2)	-0.005(9)	465(1)	12(9)	25(7)
	C	0.17(1)	0.07(1)	0.00(1)	316(1)	43(1)	52(7)

the two models, except of course for Cu and Fe, since according to model II they occupy the same site, but according to model III they have different z's. The results of the BVS calculations together with the cation-oxygen distances are listed in Table V.

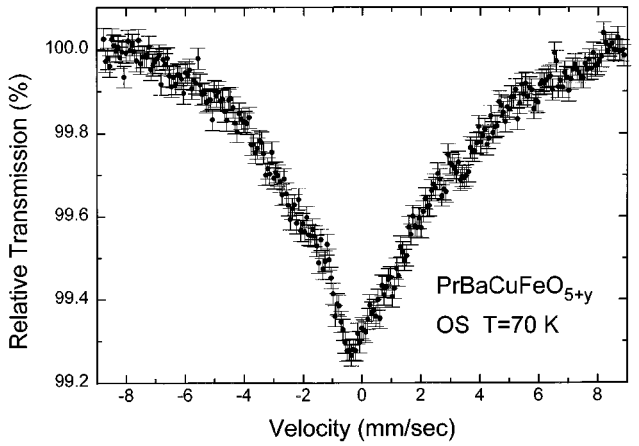

FIG. 10. Mössbauer spectra for the OS ($y\approx0.5$) $PrBaCuFeO_{5+y}$ sample at 70 K.

As oxygen is removed from the system the various atoms rearrange themselves in the unit cell. The O(2) atoms move towards the Pr layer (by ~0.05 Å) and in this way balance out the removal of the O(4) atoms, so that no change is observed in the Pr BVS. For Pr, the 3+ value means that Pr is well suited in its cage for both samples (OS and OR). The Ba atoms do not have any O(4) neighbors to account for the movement of the O(2) atoms, and so the oxygen removal causes a valence change from 2.25 (OS) to 2.05 (OR). We can deduce from these values that, for the OS sample, Ba is under stress that is relieved by the removal of the O(4) atoms. For Cu atoms, we observe a spectacular change in the BVS values from 2.80(OR) to 2.10(OS) regardless of the structural model. These values imply that for the OS sample most of the copper ($\sim80\%$) is trivalent, while for the OR sample all Cu is practically divalent. The 3+ valence of copper in the case of model II can be explained by the fact that Cu shares with Fe the same site. However, regarding model III, we believe that it just comes from the disorder of Cu and Fe in more or less the same z. The important thing about these BVS calculations is that for either models (II and III), the average valence of the (Cu,Fe) atom is 3+ for the OS sample, which assuming copper to be divalent implies that, in average, Fe is tetravalent, in accordance to the aver-

TABLE V. Selected bond lengths and calculated bond valence sums for models II and III.

Atom	Model II		Model III	
	OS	OR	OS	OR
Sr-O(1)×4	2.773	2.776	2.773	2.776
-O(2)×8	2.993(2)	3.059(6)	2.993(2)	3.065(6)
Valence	2.25(2)	2.05(2)	2.25(2)	2.03(2)
Pr-O(2)×8	2.542(1)	2.494(5)	2.542(1)	2.489(5)
-O(4)×4n	2.773	-	2.773	-
Valence	3.04(7)	3.06(9)	3.04(7)	3.10(9)
Cu-O(1)×1	2.001(2)	2.035(4)	2.03(2)	2.113(8)
-O(2)×4	1.978(1)	1.987(1)	1.974(3)	1.978(1)
-O(4)×n	1.877(2)	-	1.85(2)	-
Valence	2.78(2)	2.12(1)	2.80(5)	2.09(1)
Fe-O(1)×1	2.001(2)	2.035(4)	1.97(1)	1.895(8)
-O(2)×4	1.978(1)	1.987(1)	1.982(2)	2.016(3)
-O(4)×n	1.877(2)	-	1.91(2)	-
Valence	3.10(2)	2.63(2)	3.09(4)	2.69(3)

n equals 0.5 for the OS sample and 0 for the OR sample.

age Fe valence deduced from Mössbauer spectroscopy. Also, for the OR sample it should be noted that the average valence of the (Cu, Fe) atom is approximately 2.5+, which assuming copper to be divalent implies again that, in average, Fe is trivalent, in accordance to the Mössbauer results as well.

As in $YBaCuFeO_5$, it is Fe-O1<Fe-O2 (model III) and the values are practically the same. The average Pr-O distances are 2.59 and 2.49 Å for the OS and OR samples, respectively. In $PrBa_2Cu_3O_{7-y}$ the corresponding values are 2.45 Å for $y=0$ (that is 0.04 Å shorter than expected, provided ''normal'' Pr123 is on a straight line in the *R*-O vs ionic radius plot) and 2.48 Å for $y=1$. Unlike $PrBa_2Cu_3O_{7-y}$, in the present compound the Pr-O bond length decreases upon removing oxygen. In $PrFeO_3$ the average Pr-O distance is 2.54 Å .[18]

According to the BVS values, it turns out that $y\approx 0$ for the OR sample and $y\approx 0.6$ for the OS sample. Both values are in excellent agreement with the value obtained from the neutron data.

The cell constants and the unit cell volume increase as oxygen is removed from the structure (as in other systems such as $YBa_2Cu_3O_{7-y}$) probably due to the electrostatic repulsion between the cations which becomes larger as the intermediate (bridging) oxygen ions are removed. Alternatively, it can be explained from the decrease of the iron's valence state, but in the end this is just a consequence of the rearrangement of the various atoms. This picture is also consistent with the movement of both the Cu and Fe atoms away from the Pr layer. Especially for the *a* axis, the absence of O(4) atoms dictates to the Pr ions to move away from their initial positions in order to minimize their electrostatic repulsion.

We now turn to the probable ordering of the Pr sublattice. The assignment of the magnetic structure of the $\mathbf{k}_2$ propagation vector to the Pr sublattice is inconsistent with our data. For the first propagation vector we could explain the data supposing that the peaks come from the magnetic ordering of the Pr sublattice. However, this would require a transition temperature for the Pr sublattice as high as 380 K. Such an explanation is in disagreement with data on $PrBa_2Cu_3O_7$ and $PrBa_2Cu_3O_6$, where the Pr spins order antiferromagnetically at 17 K (Ref.19) and 11 K (Ref. 20), respectively. Moreover, for $PrFeO_3$ no magnetic transition was observed for the Pr sublattice down to 8 K (Ref. 21). It is noteworthy that the ordered magnetic moment of Fe^{3+} in the $PrFeO_3$ compound is 4.14(4) μ_B per iron at 8 K,[21] which is close to the value deduced for the oxygen reduced $PrBaCuFeO_5$ at 2 K. The reduction of the Fe^{3+} moment in $PrFeO_3$ has been attributed to a weak Pr-Fe coupling.[22]

Let us now discuss the existence of two propagation vectors in the magnetic structure of the OR sample. As discussed in the magnetic structure section it can have two explanations: (a) an *incoherent mixture of domains* or (b) a *canted model*. According to Rossat-Mignod[23] the canted model has to be considered instead of magnetic domains. The reason is that the existence of terms higher than second order in the free-energy expression can remove the degeneracy between the single and the multi-**k** structures. We could first assume that the magnetic character of Pr is exclusively responsible for the two propagation vectors. However the $YSrCuFeO_{5+y}$ compound displays a magnetic structure similar with OR $PrBaCuFeO_{5+y}$,[24] where the Y^{3+} ion (unlike Pr^{3+}) does not carry a magnetic moment. Consequently, the explanation based on Pr magnetic character is not very likely. If the O4 sites were completely empty, then only dipolar interactions would be allowed. Filling these oxygen vacancies may also give rise to superexchange interactions between the (Cu,Fe) ions above and below the Pr layer, that might explain the existence of two propagation vectors. In the case of $YBaCuFeO_{5+y}$ several transitions are observed as the temperature is lowered. Unlike $PrBaCuFeO_{5+y}$, where the extra oxygen should be responsible for the stabilization of a magnetic structure with two propagation vectors, in $YBaCuFeO_{5+y}$ the amount of the O(4) oxygen is quite small to have such an effect. So, only an incommensurate magnetic structure develops with a small contribution from $\mathbf{k}_2$.

We now turn to a discussion of the Mössbauer spectra. The first one is the presence of two components in the 433 K spectrum of the OR sample, an unexpected behavior since our structural models predict only one position for Fe. Component *A* is the structurally predicted five-fold oxygen coordinated Fe position. A first explanation of component *B* as arising from an impurity phase can be easily ruled out since both our NPD and XRD data do not reveal the existence of such a phase and especially with a $\sim$15% weight. Additional support is provided from the Mössbauer spectra, since their evolution with temperature shows that this component becomes magnetic together with component *A*. Having excluded the impurity origin of component *B*, we can attribute it to a second nonequivalent (from the Mössbauer point of view) Fe site in the structure. This can happen either with a part of Fe being octahedrally coordinated [due to some remnant O(4) oxygen] or with some Fe occupying not the

$z \simeq 0.25$ but the $z \simeq 0.27$ position, which is normally occupied by Cu. A third explanation consists in having Cu and Fe in different (successive) layers with a small amount of Fe residing at the copper plane.

The existence of two nonequivalent Fe sites, combined with fluctuations of the hyperfine parameters due to disordering effects, can explain the inhomogeneous broadening that is observed in the RT spectrum of the OR sample.

The second interesting point is that while the Mössbauer spectra for the OS sample are magnetically split, the NPD data even at 2 K do not show long-range magnetic order. The broad, magnetically split spectra close to 70 K imply that the rate of the iron spin fluctuation is comparable to the Larmor frequencies of the nuclear moment ($\sim 10^{-9}$ sec). Near 70 K the Mössbauer spectra for the OS sample might be explained by the freezing of the Fe spins (or of clusters of Fe spins) at random directions with varying local environments (because we have a variety of Fe^{3+}, Fe^{4+}, Fe^{5+}, and Cu^{2+} randomly distributed). The spins freeze randomly with respect to the c axis provided that there is no anisotropy energy. Spin freezing is also consistent with the anomaly observed around 70 K in the χ vs T curve of the OS sample.

The last question, concerning the Mössbauer spectra, is the nature of the C component. Unequivocally, it has to be related to the additional oxygen within the rare earth layer. Its hyperfine parameters suggest that it originates from Fe that is in a valence state higher than 3+, that is either 4+ or 5+. A simple charge balance calculation for the OS sample demands that, supposing Cu is divalent, all the iron should be transformed to Fe^{4+}. The unquestionable presence of Fe^{3+}, through components A and B, is the convincing evidence that component C originates from Fe atoms whose valence state is 5+.

To shed more light to the nature of C component, we are going to compare our data with those of well-studied, structurally similar compounds. The first such compound is the cubic perovskite $SrFeO_3$, a most typical case of octahedral $d^4(t_{2g}^3 e_g^1, S=2)$ high-spin Fe^{4+} configuration.[25] More complicated behavior is observed in the case of the oxygen-deficient perovskite phase $SrFeO_{3-y}$.[26] And finally, we consider $CaFeO_3$,[27] representing the case of Fe^{5+} through charge disproportionation. In order to compare the present hyperfine parameters with those of the above mentioned compounds, we will use the data at low temperatures. Assuming, that component C corresponds to Fe^{4+}, then its δ is considerably smaller than that of $SrFeO_3$, while H_{eff} is practically the same. Comparing our data with the $Fe^{(4+\lambda)}$ component of $CaFeO_3$, it can be seen that there is a very good agreement between the δ's, while H_{eff} is 37 kG greater. Therefore, our data can be explained by assigning the C component to Fe^{5+} and components A and B to Fe^{3+}, within the frame of charge disproportionation. An alternative explanation is that the C component originates from Fe ions whose electrons are delocalized, following the arguments of Gibbs regarding the Z component present in $SrFeO_{3-y}$. A component with similar isomer shift ($\delta = 0.03$ mm/s) has been observed[28] in oxygen saturated $YSr_2Cu_2FeO_{7+y}$.

At this point it is worth comparing the results of the present work with those of the RBaCuFeO$_{5+y}$ compounds discussed in Ref. 5. In that work it was established that T_N decreases with increasing y or equivalently with increasing the rare earth ionic radius. Therefore, in Pr and Nd the O4 sites are expected to have larger occupancy than the samples for rare earths with smaller ionic radius. When comparing our previous data (Ref. 5) with those of the Pr member we must take into account that the former samples were prepared by quenching of the samples from 980 °C (A series) and by heating the A-series samples in the TGA apparatus up to 900 °C (B series), whereas in the present work we have studied oxygen reduced, as-prepared and oxygen saturated samples. Thus, the OR sample can be compared with the B-series samples, the as-prepared sample with the A-series samples, but the OS sample has no equivalent. The additional site (site B) in the Mössbauer spectra of the OR sample originates from some remnant O(4) oxygen, maybe due to the large ionic radius of Pr. This is the reason we observed a paramagnetic spectrum for the AP Pr sample at RT, whereas the corresponding Nd sample (A series) shows a broad relaxed spectrum at RT.[5] Regarding the B-series Nd sample, whose equivalent is the OR sample, it has a hyperfine field of 347 kG at RT, whereas for the OR Pr sample the hyperfine field at RT is $\sim$320 kG. The absence of component B in the B series must be due to the small amount of remnant O(4) after heating in Ar. Component C was absent in the A series because it corresponds to Fe^{5+} and therefore it appears only after having exceeded a certain degree of oxygenation.

IX. SUMMARY AND CONCLUSIONS

We have studied the PrBaCuFeO$_{5+y}$ compound for different oxygen contents with x-ray and neutron powder diffraction, TGA, magnetic susceptibility, and Mössbauer spectroscopy. TGA measurements and neutron diffraction data revealed the presence of additional oxygen in the Pr layer (with occupancy 0.5 for the OS and 0.26 for the AP samples). The OR sample exhibits antiferromagnetic long-range order with $T_N = 381 \pm 5$ K, whereas for the OS sample no long-range magnetic order is observed down to 2 K obviously due to the additional oxygen within the Pr layers. The neutron diffraction data were analyzed with two propagation vectors (from 300 down to 2 K): $\mathbf{k}_1 = [\frac{1}{2}\frac{1}{2}\frac{1}{2}]$ and $\mathbf{k}_2 = [\frac{1}{2}\frac{1}{2}1]$. The magnetic structure can be interpreted by considering either a noncolinear magnetic structure or a mixture of magnetic domains, with the former being more probable. It would be very interesting to elucidate this problem by a single-crystal study. The Mössbauer spectra for the OR sample were analyzed with two Fe^{3+} ($S = 5/2$) components, while for the OS sample the extra oxygen creates holes in the (Cu, Fe) layers and as a result Fe appears in a mixed valence state. Indeed, the presence of Fe in a valence state higher than 4+ is unambiguous.

ACKNOWLEDGMENTS

Partial support for this work was provided by the E.E. through the CHRX-CT93-0116, Human Capital and Mobility Programme (access to large-scale facilities) projects and from the 89EK19 project of the Greek Secretariat for Research and Technology.

*Electronic address: pissas@cyclades.nrcps.ariadne-t.gr
†Also at Institute for Crystallography, University of Tübingen, D-72070 Tübingen, Germany.

[1] L. Er-Rakho, C. Miceli, P. Lacorre, and B. Raveau, J. Solid State Chem. **73**, 531 (1988).
[2] J. T. Voughey and K. P. Poeppelmeier, in *Proceedings of the International Conference on Chemistry of Electronic Ceramic Materials*, edited by P. K. Davies and R. S. Roth (U.S. Department of Commerce, NIST Special Publication 804, 1991), p. 419.
[3] Y. K. Atanassova, V. N. Popov, G. G. Bayachev, M. N. Iliev, C. Mitros, V. Psyharis, and M. Pissas, Phys. Rev. B **47**, 15 201 (1993).
[4] C. Meyer, F. Hartman-Boutron, Y. Gros, and P. Strobel, Solid State Commun. **76**, 163 (1990).
[5] M. Pissas, C. Mitros, G. Kallias, V. Psycharis, A. Simopoulos, A. Kostikas, and D. Niarchos, Physica C **192**, 35 (1992).
[6] A. W. Mombru, C. Christides, A. Lappas, K. Prassides, M. Pissas, C. Mitros, and D. Niarchos, Inorg. Chem. **33**, 1255 (1994).
[7] K. Prassides, C. Christides, A. Lappas, and A. Mombru (unpublished).
[8] M. Pissas, C. Mitros, G. Kallias, V. Psycharis, D. Niarchos, A. Simopoulos, A. Kostikas, C. Christides, and K. Prassides, Physica C **185-189**, 553 (1991).
[9] V. Caignaert, I. Mirebeau, F. Bouree, N. Nguyen, J-M. Greneche, and B. Raveau, J. Solid State Chem. **114**, 24 (1995).
[10] Q. Huang, P. Karen, V. L. Karen, A. Kjekshus, J. W. Lynn, A. D. Mighell, I. Natali Sora, N. Rosov, and A. Santoro, J. Solid State Chem. **108**, 80 (1994).
[11] G. Kallias, V. Psyharis, D. Niarchos, and M. Pissas, Physica C **176**, 316 (1991).
[12] D. B. Wiles and R. A. Young, J. Appl. Crystallogr. **14**, 149 (1981).
[13] J. Rodriguez-Carvajal, Physica B **192**, 55 (1993).
[14] D. Watkin, Acta Crystallogr. **A50**, 411 (1994).
[15] D. H. Lyons, T. A. Kaplan, K. Dwight, and N. Menyuk, Phys. Rev. **126**, 540 (1962); P. F. Miceli, J. M. Tarascon, L. H. Greene, P. Barboux, M. Giroud, D. A. Neumann, J. J. Rhyne, L. F. Schneemeyer, and J. V. Waszczak, Phys. Rev. B **38**, 9209 (1988); H. Kadowaki, M. Nishi, Y. Yamada, H. Takeya, H. Takei, S. M. Shapiro, and G. Shirane, *ibid.* **37**, 7932 (1988); I. Mirebeau, E. Suard, V. Caignaert, and F. Bouree, *ibid.* **50**, 3230 (1994); S. Shamoto, M. Sato, J. M. Tranquada, B. J. Sternlieb, and G. Shirane, *ibid.* **48**, 13 817 (1993).
[16] R. E. Watson and A. J. Freeman, Acta Crystallogr. **14**, 27 (1961).
[17] I. D. Brown and D. Altermatt, Acta Crystallogr. B **41**, 244 (1985).
[18] M. Marezio, J. P. Remeika, and P. D. Dernier, Acta Crystallogr. B **26**, 2008 (1970).
[19] W-H. Li, J. W. Lynn, S. Skanthakumar, T. W. Clinton, A. Kebede, C.-S. Jee, J. E. Crow, and T. Mihalisin, Phys. Rev. B **40**, 5300 (1989).
[20] M. Guillaume, P. Fischer, B. Roessli, A. Podlesnyak, J. Schefer, and A. Furrer, Solid State Commun. **88**, 57 (1993).
[21] I. Sosnowska and P. Fischer, J. Less-Common Metals **111**, 109 (1985).
[22] P. Pataud and J. Sivardieve, J. Phys. (Paris) **31**, 1017 (1970).
[23] J. Rossat-Mignod, *Methods of Experimental Physics* (Academic, New York, 1987), p.69.
[24] M. Pissas *et al.* (unpublished).
[25] P. K. Gallagher, J. B. MacChesney, and D. N. E. Buchanan, J. Chem. Phys. **41**, 2429 (1964); P. K. Gallagher, J. B. MacChesney, and D. N. E. Buchanan, *ibid.* **43**, 516 (1965); P. K. Gallagher, J. B. MacChesney, and D. N. E. Buchanan, *ibid.* **45**, 2466 (1966).
[26] T. C. Gibb, J. Chem. Soc. Dalton Trans. **4/1629**, 1455 (1985).
[27] M. Takano, N. Nakanishi, Y. Takeda, S. Naka, and T. Takada, Mater. Res. Bull. **12**, 923 (1977); Y. Takeda, S. Naka, M. Takano, T. Shinjo, T. Takada, and M. Shimada, *ibid.* **13**, 61 (1978).
[28] M. Pissas, G. Kallias, A. Simopoulos, D. Niarchos, and A. Kostikas, Phys. Rev. B **46**, 14 119 (1992); M. Pissas, G. Kallias, N. Poulakis, D. Niarchos, A. Simopoulos, and E. Liarokapis, Phys. Rev. B **52**, 10 610 (1995).